

Sub-cluster-aware Network for Few-shot Skin Disease Classification

Shuhan Li^a, Xiaomeng Li^{b,*}, Xiaowei Xu^c, Kwang-Ting Cheng^b

^aDepartment of Computer Science Engineering, Hong Kong University of Science and Technology, Clear Water Bay, Hong Kong, China

^bDepartment of Electronic and Computer Engineering, Hong Kong University of Science and Technology, Clear Water Bay, Hong Kong, China

^cGuangdong Provincial People's Hospital, Guangdong Academy of Medical Sciences, Guangdong, China

Abstract

This paper studies the few-shot skin disease classification problem. Based on a crucial observation that skin disease images often exist multiple sub-clusters within a class (i.e., the appearances of images within one class of disease vary and form multiple distinct sub-groups), we design a novel Sub-Cluster-Aware Network, namely SCAN, for rare skin disease diagnosis with enhanced accuracy. As the performance of few-shot learning highly depends on the quality of the learned feature encoder, the main principle guiding the design of SCAN is the intrinsic sub-clustered representation learning for each class so as to better describe feature distributions. Specifically, SCAN follows a dual-branch framework, where the first branch is to learn class-wise features *to distinguish different skin diseases*, and the second one aims to learn features which can effectively partition each class into several groups so as *to preserve the sub-clustered structure within each class*. To achieve the objective of the second branch, we present a cluster loss to learn image similarities via unsupervised clustering. To ensure that the samples in each sub-cluster are from the same class, we further design a purity loss to refine the unsupervised clustering results. We evaluate the proposed approach on two public datasets for few-shot skin disease classification. The experimental results validate that our framework outperforms the other state-of-the-art methods by around 2% to 4% on the SD-198 and Derm7pt datasets.

Keywords: Few-shot learning, rare skin disease classification

1. Introduction

In the past decade, advances in deep convolutional neural networks and the availability of a large amount of annotated images have continued to push the boundaries in a variety of medical image analysis tasks, such as organ segmentation (Yu et al., 2019; Taghanaki et al., 2019), tumor segmentation (Çiçek et al., 2016; Li et al., 2018; Isensee et al., 2021) and disease screening (Wang et al., 2017, 2018; Feng et al., 2020). Apart from the relatively sufficient examples of the common diseases, there are more than 6,000 known rare diseases, at much lower prevalence, affecting 7% of the population worldwide (Chung et al., 2021). The diagnosis of rare conditions for clinicians and machines has been challenging due to the lack of experiences and clinical samples. Rare skin disease diagnosis is one of the application domains that suffer from data deficiency. For example, the SD-198 dataset (Sun et al., 2016) consists of 6,584 skin images with 198 disease classes, where 70 skin classes

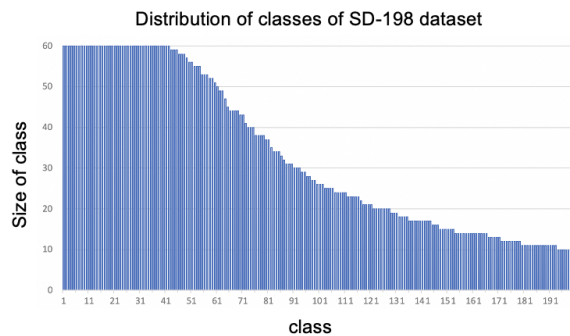


Figure 1: The long-tailed class distribution in the SD-198 dataset. The X-axis refers to 198 skin disease classes, and the Y-axis refers to the number of images in the corresponding class.

contain relatively fewer images than other skin disease cases; see Figure 1. This paper aims to develop a deep learning model which is trained with images of common skin diseases while generalizing well on rare skin diseases.

One common solution is few-shot learning (FSL), which

*Corresponding author: Xiaomeng Li (eexmli@ust.hk)

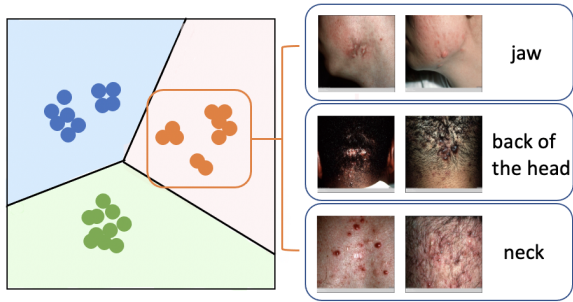


Figure 2: Left: An example of features learned by our framework. Three classes are separated by their class labels (shown in different colors), and various sub-groups are generated automatically for each class. Right: An example of a class forming three intrinsic sub-groups, with different appearances in different body parts.

aims to learn transferable knowledge on common classes (base classes) and apply it to the rare ones (novel classes) with only a handful of labeled data. Current FSL methods for few-shot skin disease classification can be broadly divided into two groups: meta-learning based (Prabhu et al., 2019; Li et al., 2020; Mahajan et al., 2020; Zhang et al., 2020; Zhu et al., 2020, 2021; Singh et al., 2021) and transfer-learning based (Guo et al., 2020; Chen et al., 2021; Medina et al., 2020; Phoo and Hariharan, 2020). In the category of meta-learning-based methods, existing solutions are mainly based on MAML (Finn et al., 2017) and Prototypical Networks (Snell et al., 2017), with the focus on different problems in rare skin disease classification. For example, Li *et al.* (Li et al., 2020) built a difficulty-aware meta-learning model based on MAML (Finn et al., 2017) to address the different weights of sampled tasks in the imbalanced skin dataset. Mahajan *et al.* (Mahajan et al., 2020) replaced the conventional convolutional layers in Reptile (Nichol et al., 2018) and Prototypical Networks (Snell et al., 2017) with group equivariant convolutions (Cohen and Welling, 2016), to obtain invariant features after different transformations. This is because skin diseases generally do not have a prevailing global orientation structure. Another line of research, i.e., transfer-learning based methods, aims to learn a powerful feature extractor in the *pre-training* stage with sufficient data, which can be quickly adapted to novel classes in the *fine-tuning* stage with a few novel examples. For example, some transfer-learning based methods focus on cross-domain few-shot learning problems (Guo et al., 2020; Chen et al., 2021; Medina et al., 2020; Phoo and Hariharan, 2020), where the images for base and novel classes belong to different domains.

Apart from the above FSL methods designed explicitly for rare skin disease classification, FSL approaches developed for

natural images can easily be adapted to this task. For example, Mangla *et al.* (Mangla et al., 2020) proposed an S2M2 framework that combines a self-supervised loss with manifold-mixup techniques to train a rich and robust feature extractor. Liu *et al.* (Liu et al., 2020) introduced a NegMargin method which applies a Softmax loss with a negative margin to train the encoder, achieving a better result on novel classes than using the regular Softmax loss. However, we find that the performance achieved by these methods on skin disease datasets is limited; see the results of S2M2 (Mangla et al., 2020) and NegMargin (Liu et al., 2020) in Table 1, Table 2 and Table 3. We argue that one limitation of the current FSL methods is that they aim to learn a class-wise discriminative feature encoder, which minimizes the intra-class distances and enlarges the inter-class distances. However, this does not match the intrinsic distribution in skin conditions, where each type of disease may contain sub-clustered structures.

In contrast to natural images, skin disease images show the existence of multiple latent groups within a class, i.e., sub-clusters. For example, the same type of skin disease may occur on different body parts (e.g., jaw, neck, or back of the head), leading to the intrinsic sub-clustered structures for the same skin disease. For example, for a specific skin disease, some cases are detected on the jaw while other cases occur on the neck, as shown in Figure 2, and thus their appearances may vary. As the performance of few-shot learning highly depends on the learned feature encoders, the main objective of this paper is to enhance the feature representation by discovering the intrinsic sub-clusters in the base classes. Therefore, we design a novel dual-branch Sub-Cluster-Aware Network, namely SCAN, which can identify the intrinsic sub-clustered structures in the skin disease datasets. By learning intrinsic sub-clustered structures in skin images, the network is expected to learn better feature representation from base classes. This can then improve the performance on the novel classes. Specifically, in addition to learning the class-wise features *to distinguish different skin diseases*, SCAN learns sub-clustered features within each class *to preserve sub-clustered structure within each class*. To achieve intrinsic sub-clustered representation learning, we present a clustering branch with cluster loss to learn image similarities via unsupervised clustering. To ensure that the samples in each sub-cluster are from the same class, we further design a purity loss to refine the unsupervised clustering results. Notably, our framework can automatically determine the number of groups for each class, i.e., various cluster numbers are learned according to different class distributions. In the fine-tuning stage, we evaluate the performance of the pre-trained encoder on novel classes with sampled episodes.

Experimental results on two skin disease benchmark

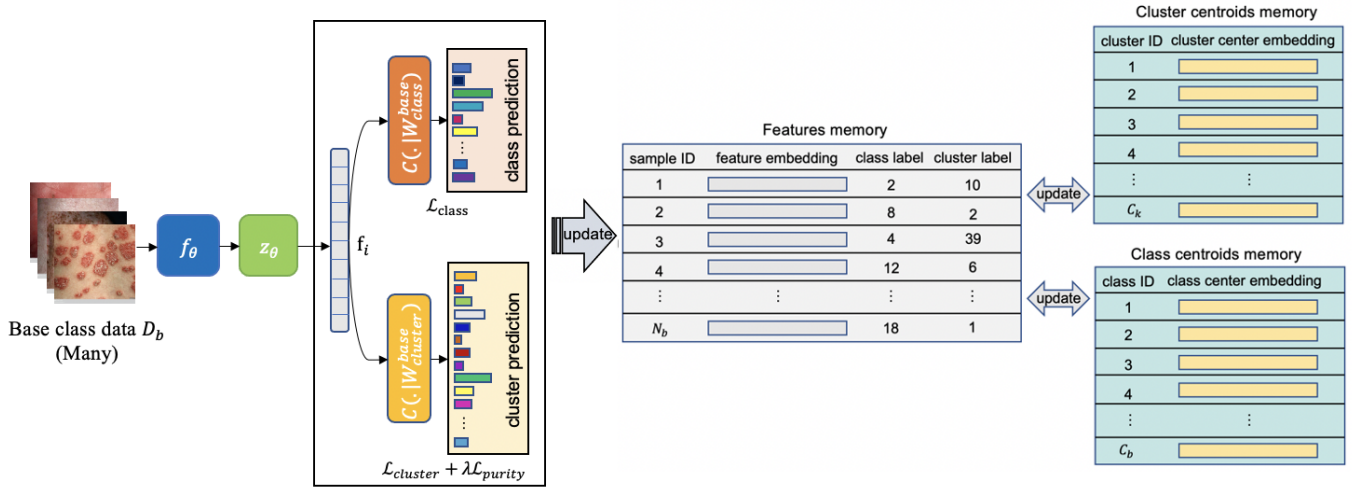


Figure 3: Overview of proposed Sub-Cluster-Aware Network (SCAN). We train this network on base class data in pre-training stage.

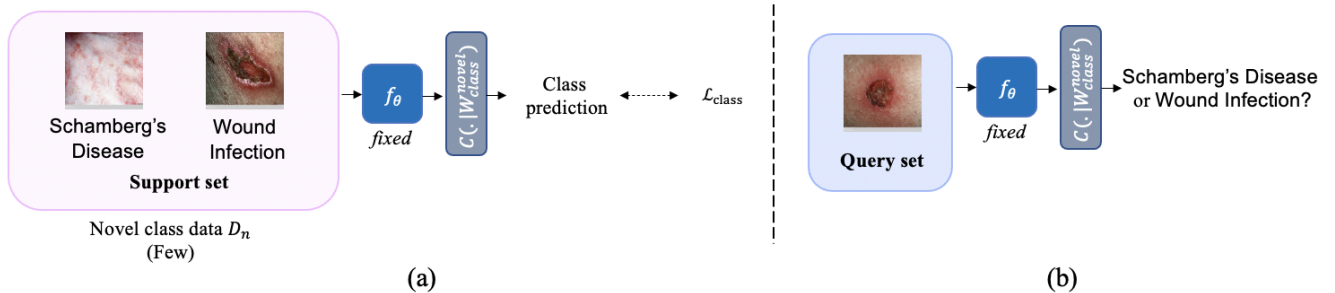


Figure 4: An example of fine-tuning stage for a 2-way 1-shot task on novel class set. We utilize the feature encoder f_θ trained in the pre-training stage and fix the parameters. (a): In each episode, a classifier is trained by support set images. (b): Evaluating on query set images.

datasets, SD-198 (Sun et al., 2016) and Derm7pt (Kawahara et al., 2018), show that our method outperforms prior art. In summary, our contributions can be summarized as follows:

- We present a dual-branch framework for rare skin disease classification with the critical motivation of identifying the sub-clusters in each disease class.
- A powerful feature encoder is developed by this dual-branch framework. It integrates supervised classification (class branch) and unsupervised clustering (clustering branch) in the pre-training stage.
- We propose a purity loss to improve the result of intra-class clustering in the unsupervised clustering branch.
- Our method is evaluated on two public skin disease datasets, SD-198 (Sun et al., 2016) and Derm7pt (Kawahara et al., 2018), and achieves state-of-the-art results for

few-shot skin disease classification. Code is available at <https://github.com/xmed-lab/SCAN>.

2. Related works

2.1. Few-shot Learning in Computer Vision

Few-shot learning (FSL) aims to acquire prior knowledge from the base classes (with large labeled examples) and propagates it to the novel classes (with insufficient labeled examples, unseen during the training stage). Approaches can be classified into two groups according to different training processes, namely meta-learning and transfer-learning based methods. Motivated by meta-learning, several early works of FSL (Finn et al., 2017; Nichol et al., 2018; Vinyals et al., 2016; Snell et al., 2017; Sung et al., 2018; Yuan et al., 2020) can be grouped into the meta-learning class, which episodically trains the model

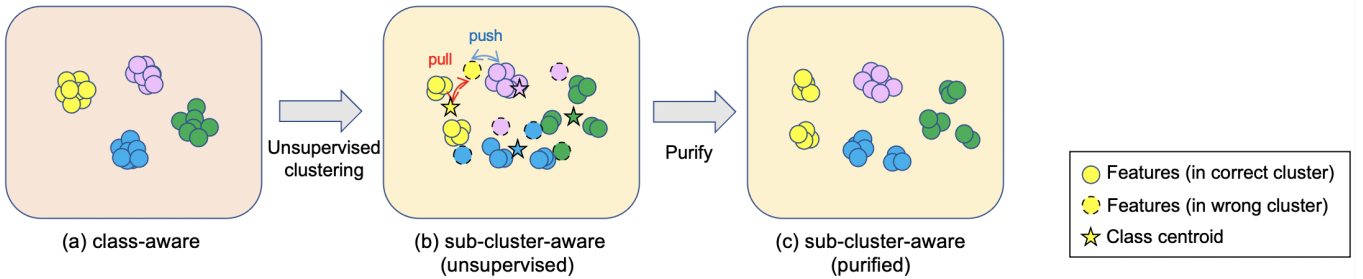


Figure 5: Effects of cluster loss $\mathcal{L}_{cluster}$ (from (a) to (b)) and purity loss \mathcal{L}_{purity} (from (b) to (c)).

to learn how to update the network with a few sampled examples. It can therefore achieve promising accuracy on the novel classes with very little labeled data. Meta-learning based methods can be further classified into two branches, one is the so-called gradient-based methods, such as MAML (Finn et al., 2017), and Reptile (Nichol et al., 2018), which are dedicated to learning good initialization parameters for every episode. They can quickly be adapted to the unseen classes within one or a few steps of gradient descending updates. Another branch, named metric-based methods, utilizes the encoded feature vectors and applies a distance metric between training and test images to assign the labels according to the nearest neighbor principle. The metric can be cosine similarity (e.g., Matching Networks (Vinyals et al., 2016)), or Euclidean distance (e.g., Prototypical Networks (Snell et al., 2017)). Recently, several works (Chen et al., 2019; Dhillon et al., 2019; Tian et al., 2020) proposed a new model which has become transfer-learning based methods. A standard classification network is trained on base classes while the classifier head is fine-tuned on the episodes generated from the novel classes. Note that we regard this model as the baseline of our proposed method. This category of algorithm aims to learn a strong feature extractor to generate transferable features on novel set so that just a fine-tuned classifier can suffice to achieve acceptable results. Experiments show that the baseline of transfer-learning based methods, i.e., a classification network trained with standard cross-entropy loss, can achieve a comparable performance against previous methods with a more simpler and more effective process (Chen et al., 2019; Wang et al., 2019). Owing to the superior performance of transfer-learning based methods, we explore them as ways to predict rare skin diseases.

2.2. Few-shot Learning for Skin Disease Classification

Due to the unbalanced distribution of skin disease classes and the deficient images of rare conditions, it is essential to apply few-shot learning methods to alleviate the reliance on massive training data. In the group of meta-learning based

methods, Li *et al.* (Li et al., 2020) built a Difficulty-Aware Meta-Learning method (DAML) based on MAML, which considers various difficulties in different episodic tasks. The model adjusts the weights of task-specific losses by down-weighting the easy tasks and increasing the hard ones so that easier tasks become less important and harder tasks more dominant. In (Singh et al., 2021), Singh *et al.* trained the Reptile model along with some advanced data augmentation techniques like mixup, cutout, cutmix as the regularization term, and increase the model generalization ability by 2%~5%.

There are more works that have been proposed based on the algorithms in the metric-based category. Mahajan *et al.* (Mahajan et al., 2020) replaced the conventional CNN with Group Equivariant Convolutions (Cohen and Welling, 2016) due to the rotation invariant of skin disease images. Zhu *et al.* (Zhu et al., 2020) indicated the incompatibility between cross-entropy loss and episode training, and proposed query-relative loss to further enhance the behavior. Another work, Zhu *et al.* (Zhu et al., 2021) built upon Prototypical Networks which can implicitly generate prototypes for each episode. They set different temperature for different categories to penalize query samples that are not close enough to their belonging categories to further strengthen the generalization ability of the learned metric.

For the category of transfer-learning based algorithms, there is no sufficient work designed for rare skin disease diagnosis. Instead, people focus on another topic, namely cross-domain FSL (Guo et al., 2020), which pre-trains the model on Imagenet and fine-tunes on unseen classes, e.g., skin lesion dataset. Considering the domain shift problem under this setting, some works (Chen et al., 2021; Medina et al., 2020; Phoo and Hariharan, 2020) brought in unlabeled data from the target domain and self-supervised learning to mitigate the performance degradation of few-shot learners. This is due to large source and target domain differences. However, different from previous researches, we mainly focus on rare skin disease classification which still remains to be explored.

Nevertheless, few methods think over the sub-cluster struc-

tures within skin disease class, except for Prototypical Clustering Networks (PCN) proposed by Prabhu *et al.* (Prabhu et al., 2019). They extend Prototypical Networks by representing each class as multiple prototypes, instead of a single one. However, PCN divides each class into fixed k sub-clusters which is reckoned without particular clustering results among classes. Compared to PCN, our designed framework can learn the specific intrinsic sub-clusters for each skin disease type, and hence, generate more accurate feature representations for transference to unseen classes.

3. Methodology

3.1. Problem Setting

In few-shot learning, data are partitioned into two disjoint sets: the base class set and the novel class set. We denote the images from the base class set as $D_b = \{(x_i, y_i)\}_{i=1}^{N_b}$, which contains N_b labeled images from C_b base classes and $y_i \in \{1, \dots, C_b\}$. Let $D_n = \{(x_i, y_i)\}_{i=1}^{N_n}$ denote the image dataset of the novel class, with few samples from C_n classes, where $C_b \cap C_n = \emptyset$. The main goal of few-shot skin disease classification is to learn rich and transferable feature representations from the base set, such that they can easily be adapted to the novel set with only a few labeled data.

To evaluate the generalization ability on the unseen classes, we sample N -way K -shot episodes from novel set D_n following the most common way proposed by Vinyals *et al.* (Vinyals et al., 2016). Each episode contains a *support set* for fast adaptation and a *query set* for model evaluation. In the support set, N classes are randomly selected from C_n novel classes and K labeled images are sampled from each class, denoted as $S = \{(x_i, y_i)\}_{i=1}^{N \times K}$. In the query set, q images are picked from the same N classes without their labels, denoted as $Q = \{(x_i)\}_{i=1}^{N \times q}$. The label information of query set Q is only available when computing the accuracy.

Our work is based on the transfer-learning few-shot learning paradigm. Therefore, we train a feature encoder in the pre-training stage with the data from the base set, as shown in Figure 3. Then, we reserve the feature extractor f_θ of the trained model and freeze the network parameters. In the following fine-tuning stage, we fine-tune a new classifier by using the images from the support set in a sampled episode, and evaluate the accuracy on the query set, as shown in Figure 4.

3.2. Framework Overview

To specifically identify the sub-clusters within each class, we design the Sub-Cluster-Aware Network (SCAN) in the pre-training stage. The overall framework is shown in Figure 3,

which consists of a dual-branch network structure as well as several auxiliary memory banks.

The dual-branch network includes a feature extractor f_θ for feature encoding, a projection head z_θ for dimensional reduction, and two linear classifiers $C(\cdot | \mathbf{W}_{class}^{base})$, $C(\cdot | \mathbf{W}_{cluster}^{base})$ for class and cluster prediction, respectively. We train the network using the labeled data in base classes by minimizing three losses: \mathcal{L}_{class} , $\mathcal{L}_{cluster}$ and \mathcal{L}_{purity} . \mathcal{L}_{class} is a standard cross-entropy loss computed for the class branch, which aims to classify skin disease according to the class labels. The other two losses are used in the cluster branch, with more details introduced below.

3.3. Sub-Cluster-Aware Network

Due to the intrinsic sub-cluster structure in the skin disease datasets, the model trained with the class-wise cross-entropy loss cannot learn the structural relationships **within** a skin disease class, as shown in Figure 5(a). Considering the sub-cluster structure for skin disease images, we present a novel Sub-Cluster-Aware Network (SCAN) to learn sub-cluster embeddings for skin disease classification.

To achieve this, we create three memory banks, i.e., feature memory, class centroid memory, and cluster centroid memory; as shown in Figure 3. The feature memory bank contains the feature embeddings and their class and cluster labels. The cluster labels are the psudeo-labels predicted by the cluster classifier head $C(\cdot | \mathbf{W}_{cluster}^{base})$ and they are initialized by K-Means. The size of the feature memory bank is set as N_b , i.e., the total number of training images, and the total cluster number selected for K-Means depends on the dataset. The class centroid memory saves the center embedding of each class by averaging all the features from the corresponding class. The size of the class centroid memory bank is set to the total number of classes in the base class dataset. Similar to the class centroid memory, the cluster centroid memory stores the mean feature of each cluster, and the size is the number of total clusters.

Then, in each forward propagation, the network and memory banks are updated through the procedures in the following sections.

3.3.1. Forward propagation

We derive the feature embedding $\mathbf{f}_i = z_\theta(f_\theta(x_i)) \in \mathbb{R}^d$ for an input image x_i , where d refers to the dimension of \mathbf{f}_i . After sending \mathbf{f}_i to two classifiers, we obtain the class probability prediction $p_i \in \mathbb{R}^{C_b}$ and the cluster probability prediction $p'_i \in \mathbb{R}^{C_k}$, correspondingly. Here, C_b is the number of base classes and C_k is the number of clusters. We set $C_k > C_b$ such that the model can acquire the finer structures than the original granularity defined by the class labels.

Table 1: 2-way 1-shot and 2-way 5-shot few-shot classification results (%) on the SD-198 dataset. Results of other methods are produced by our re-implementation. †Results reported in the paper. “-” refers to not reported in the paper.

Method	Backbone	2-way 1-shot		2-way 5-shot	
		Accuracy	F1-score	Accuracy	F1-score
PCN (Prabhu et al., 2019)	Conv4	70.03±1.42	70.78±1.61	84.95±1.15	85.87±1.12
SCAN (ours)		77.12±1.44	78.00±1.51	90.22±0.95	91.01±0.90
Meta-derm (Mahajan et al., 2020)	Conv6	65.3 [†]	-	83.7 [†]	-
SCAN (ours)		76.75±1.42	77.64±1.50	87.45±1.08	88.28±1.03
NCA (Wu et al., 2018)	WRN-28-10	71.27±1.50	71.27±1.50	83.30±1.20	84.23±1.19
Baseline (Chen et al., 2019)		75.72±1.47	76.64±1.56	88.95±1.00	89.66±0.97
S2M2_R (Mangla et al., 2020)		76.42±1.52	77.51±1.59	90.32±0.89	90.97±0.89
NegMargin (Liu et al., 2020)		76.85±1.39	77.98±1.45	89.92±0.96	90.65±0.92
SCAN (ours)		80.20±1.44	81.21±1.46	91.48±0.88	92.08±0.85

Table 2: 5-way 1-shot and 5-way 5-shot few-shot classification results (%) on the SD-198 dataset. Results of other methods are produced by our re-implementation. †Results reported in the paper. “-” refers to not reported in the paper.

Method	Backbone	5-way 1-shot		5-way 5-shot	
		Accuracy	F1-score	Accuracy	F1-score
PCN (Prabhu et al., 2019)	Conv4	77.92±0.38	45.59±1.03	85.91±0.39	65.70±1.02
SCAN (ours)		81.85±0.41	55.60±1.07	89.79±0.34	75.65±0.87
Meta-derm (Mahajan et al., 2020)	Conv6	-	-	-	-
SCAN (ours)		81.37±0.42	54.07±1.24	89.53±0.36	74.73±0.92
NCA (Wu et al., 2018)	WRN-28-10	78.17±0.41	45.91±1.08	84.73±0.38	62.83±1.01
Baseline (Chen et al., 2019)		80.63±0.42	52.54±1.11	89.46±0.38	74.71±0.96
S2M2_R (Mangla et al., 2020)		81.91±0.43	55.49±1.13	90.84±0.33	78.17±0.84
NegMargin (Liu et al., 2020)		82.15±0.43	56.04±1.14	90.68±0.35	77.75±0.87
SCAN (ours)		83.23±0.44	58.75±1.14	92.16±0.31	81.43±0.77

3.3.2. Computing class loss \mathcal{L}_{class}

A standard cross-entropy loss in Eq. 1 is used to compute class loss \mathcal{L}_{class} :

$$\mathcal{L}_{class} = \frac{1}{N_b} \sum_{i=1}^{N_b} \sum_{c=1}^{C_b} -y_{i,c} \log p_{i,c}, \quad (1)$$

$$y_{i,c} = \mathbb{1}[y_i = c], \quad (2)$$

where N_b denotes the amount of training data in base classes, and $\mathbb{1}(\cdot)$ is the indicator function. $y_{i,c}$ is equal to 1 if c is the correct class label of input image x_i , otherwise, $y_{i,c}$ is equal to 0. $p_{i,c}$ denotes the c_{th} item in the class probability vector p_i which represents the probability of x_i predicted as class c .

3.3.3. Computing cluster loss $\mathcal{L}_{cluster}$

With the cluster label of feature \mathbf{f}_i recorded in the feature memory, denoted as y'_i , we calculate the cluster loss $\mathcal{L}_{cluster}$ by

Eq. 3:

$$\mathcal{L}_{cluster} = \frac{1}{N_b} \sum_{i=1}^{N_b} \sum_{s=1}^{C_k} -y'_{i,s} \log p'_{i,s}, \quad (3)$$

$$y'_{i,s} = \mathbb{1}[y'_i = s], \quad (4)$$

Similarly, $y'_{i,s}$ is equal to 1 if s is the cluster label of input image x_i , otherwise $y'_{i,s}$ is 0. $p'_{i,s}$ denotes the cluster probability of x_i predicted as cluster s .

3.3.4. Computing purity loss \mathcal{L}_{purity}

With the restrictions of the above two losses, \mathcal{L}_{class} and $\mathcal{L}_{cluster}$, the features can form the sub-cluster structure to a certain extent. However, the clustering may not precisely occur within the class as the class labels are not utilized during cluster prediction. Samples from different classes are likely to be wrongly gathered into the same cluster because of the inter-class similarity, as shown in Figure 5(b). In order to correct

Table 3: 2-way 1-shot and 2-way 5-shot few-shot classification results (%) on the Derm7pt dataset. Results of other methods are produced by our re-implementation. †Results reported in the paper.

Method	Backbone	2-way 1-shot		2-way 5-shot	
		Accuracy	F1-score	Accuracy	F1-score
PCN (Prabhu et al., 2019)	Conv4	59.98±1.28	58.54±1.63	70.62±1.38	71.85±1.48
SCAN (ours)		61.42±1.49	61.90±1.66	72.58±1.28	74.05±1.32
Meta-derm (Mahajan et al., 2020)	Conv6	61.8 [†]	-	76.9 [†]	-
SCAN (ours)		62.80±1.34	63.75±1.50	76.65±1.21	73.60±1.25
NCA (Wu et al., 2018)	WRN-28-10	56.32±1.29	56.41±1.46	67.18±1.15	68.13±1.22
Baseline (Chen et al., 2019)		59.43±1.34	59.61±1.50	74.28±1.14	75.26±1.17
S2M2_R (Mangla et al., 2020)		61.37±1.33	61.52±1.52	79.83±1.34	80.69±1.36
NegMargin (Liu et al., 2020)		58.00±1.44	57.50±1.65	70.12±1.30	71.07±1.36
SCAN (ours)		65.27±1.38	66.35±1.49	77.97±1.27	79.16±1.28

the improper clustering results, we design a purity loss \mathcal{L}_{purity} (Eq. 5) to refine the clusters:

$$\begin{aligned} \mathcal{L}_{purity} &= \sum_{i=1}^{N_b} \mathcal{L}_{triplet}(\mathbf{f}_i, \mathbf{f}_i^p, \mathbf{f}_i^n) \\ &= \sum_{i=1}^{N_b} \max(\|\mathbf{f}_i - \mathbf{f}_i^p\|_2^2 - \|\mathbf{f}_i - \mathbf{f}_i^n\|_2^2 + \alpha, 0), \end{aligned} \quad (5)$$

where \mathbf{f}_i is the anchor, the positive sample \mathbf{f}_i^p is the class center of the anchor’s class, the negative sample \mathbf{f}_i^n is the nearest feature in the same cluster of \mathbf{f}_i with a different class label, and α denotes the margin between positive and negative pairs. Hence, if the distance between anchor and positive item is longer than the distance between the anchor and negative sample by a margin α , the purity loss \mathcal{L}_{purity} will take effect, as shown in Figure 5(c). The anchor will be pushed away from the wrong cluster and be pulled towards its correct class when minimizing \mathcal{L}_{purity} .

3.3.5. Updating memory banks

Finally, we update the contents in three memory banks according to the feature embeddings in the current epoch for the usage of next iteration.

In the feature memory bank, we smoothly update feature embeddings with a momentum decay rate $\beta \in (0, 1]$:

$$\mathbf{f}_{m,i} \leftarrow \beta \frac{\mathbf{f}_i}{\|\mathbf{f}_i\|} + (1 - \beta)\mathbf{f}_{m,i}, \quad (6)$$

where \mathbf{f}_i is the feature embedding with sample ID $i \in \{1, 2, \dots, N_b\}$, and $\mathbf{f}_{m,i}$ represents the feature saved at the i th location in the features memory bank. The cluster label is assigned to item i according to the nearest cluster center. The class labels

remain the same since the ground truth does not change during training. In the class centroid memory bank, the centers of all the classes $c_i \in C_b$ are recalculated by the updated embeddings in the feature memory bank. In the cluster centroid memory bank, the centers of all the cluster $s_i \in C_k$ are recalculated by the updated embeddings and cluster labels.

To sum up, the whole loss function (Eq. 7) of our proposed SCAN framework is the summation of three parts:

$$\mathcal{L}_{SCAN} = \mathcal{L}_{class} + \mathcal{L}_{cluster} + \lambda \mathcal{L}_{purity}, \quad (7)$$

where λ is the weight for purity loss.

4. Experiments

4.1. Datasets

SD-198 dataset (Sun et al., 2016) consists of 6,584 clinical images captured by mobile phones or digital cameras from 198 skin disease classes, with 10 to 60 examples in each category. The images differ in color, exposure, and illumination, and contain a wide range of patients of different age, gender, skin color, disease location and duration. To fairly compare with existing methods, we follow previous work (Mahajan et al., 2020) to split the dataset into base and novel sets: 20 classes with 60 images per class compose the base set, and 70 classes with less than 20 examples per class form the novel set.

Derm7pt dataset (Kawahara et al., 2018) includes more than 2,000 color images from 20 skin lesion classes. Following previous work (Mahajan et al., 2020), we exclude two classes: “miscellaneous” and “melanoma”, and split the remaining 18 classes into base and novel sets according to their settings: 13 classes of larger size are selected as the base set, and the remaining 5 classes with the minimum amount of images are the novel set.

Table 4: Existing state-of-the-art FSL methods can be enhanced with our proposed SCA branch. Results (%) on the SD-198 dataset with 2-way 1-shot and 2-way 5-shot settings. (Backbone: WRN-28-10).

Method	2-way 1-shot		2-way 5-shot	
	Accuracy	F1-score	Accuracy	F1-score
S2M2_R (Mangla et al., 2020)	76.42±1.52	77.51±1.59	90.32±0.89	90.97±0.89
S2M2_R+SCAN (ours)	79.23±1.41	80.27±1.44	91.00±0.90	91.60±0.88
NegMargin (Liu et al., 2020)	76.85±1.39	77.98±1.45	89.92±0.96	90.65±0.92
NegMargin+SCAN (ours)	78.60±1.44	79.79±1.46	91.43±0.90	92.07±0.85

Table 5: Existing state-of-the-art FSL methods can be enhanced with our proposed SCA branch. Results (%) on the SD-198 dataset with 5-way 1-shot and 5-way 5-shot settings. (Backbone: WRN-28-10).

Method	5-way 1-shot		5-way 5-shot	
	Accuracy	F1-score	Accuracy	F1-score
S2M2_R (Mangla et al., 2020)	81.91±0.43	55.49±1.13	90.84±0.33	78.17±0.84
S2M2_R+SCAN (ours)	82.94±0.43	58.10±1.14	91.28±0.33	79.58±0.80
NegMargin (Liu et al., 2020)	82.15±0.43	56.04±1.14	90.68±0.35	77.75±0.87
NegMargin+SCAN (ours)	83.67±0.43	60.03±1.16	92.33±0.33	81.95±0.80

We resize all the input images to 80×80 for the above two datasets and apply the standard augmentations such as random cropping, color jittering, rotation (-30 degrees to +30 degrees), and horizontal flipping.

4.2. Implementation Details

To fairly compare with existing few-shot methods, we employ **Conv4**, **Conv6** (Snell et al., 2017), and **Wide ResNet (WRN)** (Zagoruyko and Komodakis, 2016) as backbones. To show the flexibility of our method, we further integrate our SCAN framework with **ResNet18** and **ResNet34** (He et al., 2016). For the projection head z_θ , we use a non-linear structure [fc – bn – relu – dropout – fc – relu], which reduces the feature embedding dimensions to 256. Both classifiers $C(\cdot|\mathbf{W}_{class}^{base})$ and $C(\cdot|\mathbf{W}_{cluster}^{base})$ have the same structure, i.e., a fully connected layer followed by a Softmax function. The number of classes C_b is 20 for SD-198 and 13 for Derm7pt while the number of cluster C_k is set to 50 and 40, respectively. For the hyperparameters in loss functions, we set α in Eq. 5 as 0.3, β in Eq. 6 as 0.5, and λ in Eq. 7 as 1. To train our SCAN model, we set the batch size to 16 and 64 for the SD-198 and Derm7pt datasets, respectively. We choose the SGD optimizer with a 0.0075 learning rate, 0.9 momentum and 10^{-5} weight decay for 800 epochs training.

To evaluate the performance on the novel set D_n , we freeze the parameters of the feature extractor f_θ and use it to encode images in the novel set to feature embeddings. Episodes

are generated from the novel set randomly. We set 2-way 1-shot, 2-way 5-shot, 5-way 1-shot and 5-way 5-shot for SD-198 dataset, and set 2-way 1-shot and 2-way 5-shot for the Derm7pt dataset. 5 query images are selected in each episode for both two datasets. For each episode, we train an episodic-specific linear classifier on the support set with the augmentation techniques introduced in (Yang et al., 2021), and test the average accuracy and the F1-score on the query set. The final results are reported as the mean classification result over 600 randomly sampled episodes with 95 confidence intervals.

4.3. Results

4.3.1. Results on SD-198 dataset

The results of our proposed SCAN approach together with several other different methods on the SD-198 dataset are reported in Tables 1 and 2. Among the compared methods, PCN (Prabhu et al., 2019) and Meta-derm (Mahajan et al., 2020) are two meta-learning based FSL algorithms designed for rare skin disease classification. Meta-derm (Mahajan et al., 2020) is built on Reptile and ProtoNets by using a substitute Group Equivariant Convolutions, and they present the state-of-the-art accuracy on the SD-198 dataset with 2-way 1-shot and 5-shot settings. However, they ignore the large intra-class variation issue for skin diseases, therefore our method exceeds the accuracy of the SOTA method by around 9% and 4% in 1-shot and 5-shot experiments, respectively. In PCN (Prabhu et al., 2019), similar to us, the sub-cluster structure for each skin disease type

Table 6: The accuracy (%) performance of various backbones on the SD-198 dataset for 2-way and 5-way classification tasks.

Method	Backbone	2-way 1-shot	2-way 5-shot	5-way 1-shot	5-way 5-shot
Baseline (Chen et al., 2019)	Conv4	73.98±1.38	88.67±1.01	80.62±0.41	89.40±0.36
SCAN (ours)		77.12±1.44	90.22±0.95	81.85±0.41	89.79±0.34
Baseline (Chen et al., 2019)	Conv6	73.48±1.43	86.35±1.08	80.03±0.42	87.63±0.37
SCAN (ours)		76.75±1.42	87.45±1.08	81.37±0.42	89.53±0.36
Baseline (Chen et al., 2019)	ResNet18	71.52±1.45	84.22±1.15	78.95±0.41	86.87±0.37
SCAN (ours)		73.57±1.53	85.83±1.13	80.19±0.40	88.30±0.34
Baseline (Chen et al., 2019)	ResNet34	71.92±1.45	84.53±1.17	78.83±0.40	86.80±0.37
SCAN (ours)		73.08±1.42	85.03±1.12	79.54±0.42	87.45±0.40
Baseline (Chen et al., 2019)	WRN-28-10	75.72±1.47	88.95±1.00	80.63±0.42	89.46±0.38
SCAN (ours)		80.20±1.44	91.48±0.88	83.23±0.44	92.16±0.31

Table 7: Effect of three components of SCAN on few-shot classification accuracy (%) and intra-class cluster error rate on SD-198 dataset.

Class branch (\mathcal{L}_{class})	Clustering branch ($+\mathcal{L}_{cluster}$)	Clustering branch ($+\mathcal{L}_{purity}$)	2-way 1-shot	2-way 5-shot	5-way 1-shot	5-way 5-shot	Cluster Error Rate
✓			75.72±1.47	88.95±1.00	80.63±0.42	89.46±0.38	-
✓	✓		78.65±1.46	89.46±0.98	81.29±0.42	90.88±0.37	35.10
✓	✓	✓	80.20±1.44	91.48±0.88	83.23±0.44	92.16±0.31	20.58

is taken into account, but each class is partitioned into fixed k sub-clusters without considering the unique distributions of different classes. Unlike them, we consider intra-class diversity problem in skin disease datasets and propose SCAN to recognize better sub-cluster structures for each disease type, and hence, we improve the accuracy by 7% for a 2-way 5-shot setting and 10% for the other three settings. Also, there are similar improvements for other evaluation metrics.

To show the outstanding performance of SCAN not only compared to meta-learning based methods, we also conduct comparison experiments on several state-of-the-art transfer-learning based FSL methods. To the best of our knowledge, no previous works apply the same training procedure on rare skin disease diagnosis. Therefore, we select four transfer-learning based algorithms proposed for natural images and test their results on our datasets. NCA (Wu et al., 2018) implements neighbor component analysis in the loss which can learn the relationships between features. The baseline (Chen et al., 2019) was proposed as the baseline model for transfer-learning based FSL methods. It trains the feature encoder with a standard cross-entropy loss. S2M2_R (Mangla et al., 2020) utilizes self-supervision and Manifold Mixup to enhance the feature encoder. NegMargin (Liu et al., 2020) applies negative margin softmax loss during training and obtains increased results during evaluation. Compared to them, our SCAN algorithm pays

attention to the sub-cluster structures in skin disease datasets which are not considered by these methods. The results show that our method achieves the best performance among several state-of-the-art transfer-learning based algorithms.

4.3.2. Results on Derm7pt dataset

The results of our proposed SCAN method and other related works on the Derm7pt dataset are presented in Table 3. Similar to the SD-198 dataset, we compare our method to the state-of-the-art meta-learning and transfer-learning based FSL methods. In general, the experimental results show that our method provides the superior performance on the Derm7pt dataset among all the compared algorithms in a 2-way 1-shot setting. It also achieves competitive results compared to the state-of-the-art methods in a 2-way 5-shot setting. For the reason that our method obtains less improvement on the Derm7pt dataset than the SD-198 dataset, we speculate that the sub-cluster structures in the Derm7pt dataset may not be obvious. Hence, it is hard for SCAN to maximize its advantages.

4.3.3. Plug-and-Play module

Our SCAN framework can be used as a plug-and-play branch to enhance existing FSL methods. We validate the performance by combining the cluster branch of SCAN with two

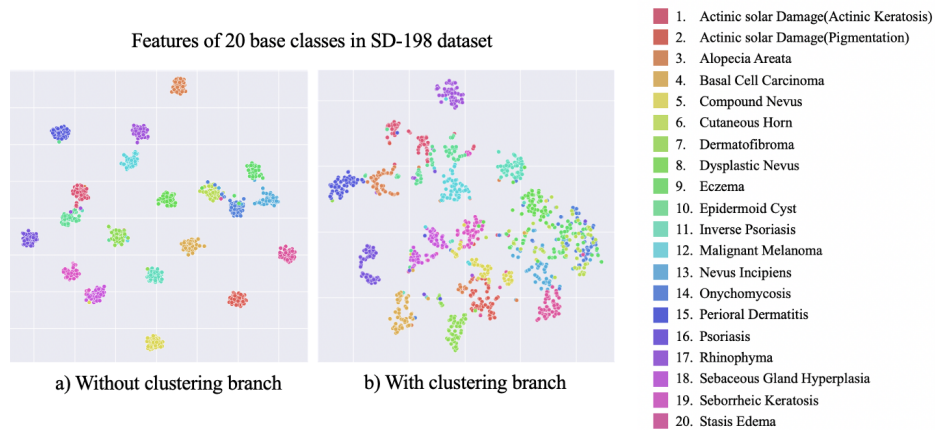


Figure 6: Impact of clustering branch on features in the base classes of SD-198 dataset. The t-SNE visualization results of 20 base classes are shown in a) without clustering branch and b) with clustering branch respectively.

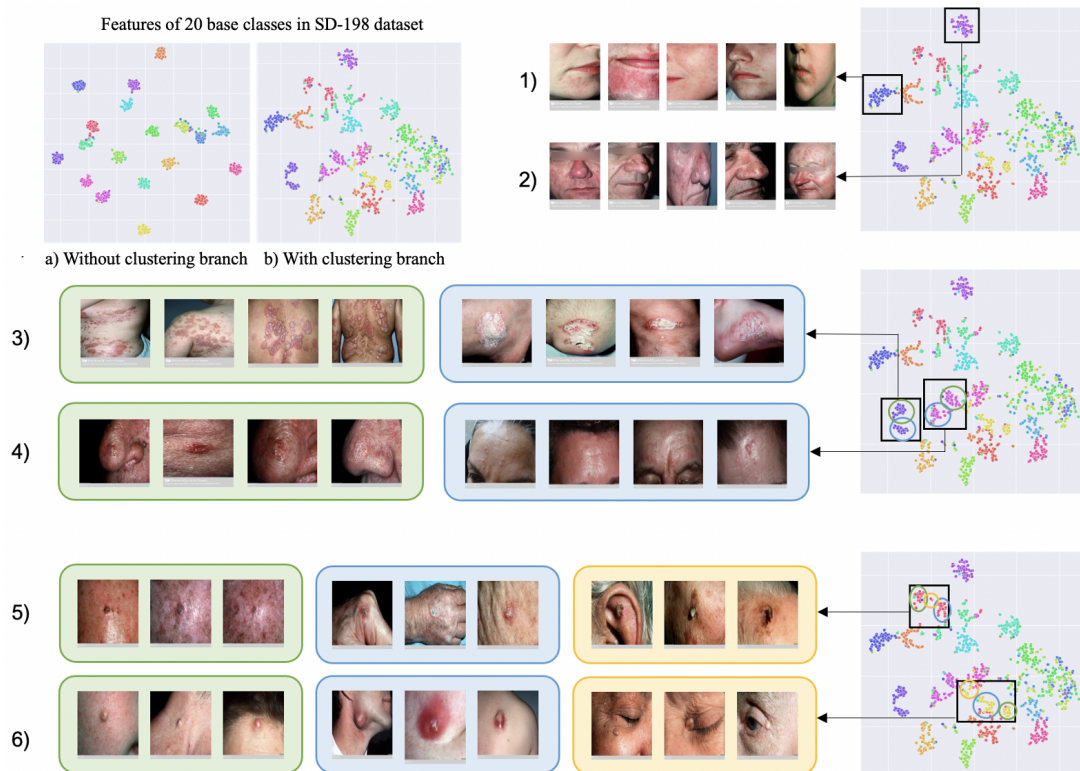


Figure 7: Examples of sub-clusters developed by SCAN. Top left: The t-SNE visualization results. Top right, middle and bottom: Examples of the various numbers of sub-clusters learned by SCAN: One sub-cluster classes: 1) Perioral Dermatitis, 2) Rhinophyma; Two sub-clusters classes: 3) Psoriasis, 4) Sebaceous Gland Hyperplasia; Three sub-clusters classes: 5) Actinic Solar Damage(Actinic Keratosis), 6) Epidermoid Cyst.



Figure 8: Results of query images prediction on the SD-198 novel set for 5-way 1-shot task. (1) (2) (3) are sampled episodes. For each episode, in the top row are images from the support set. There are 5 classes in total and 1 image from each class. The remaining 5 images are the query images from one of the above 5 classes in the support set, and we use a yellow bounding box to show the target class. Three rows show the testing results of three methods: (a) Baseline (Chen et al., 2019), (b) PCN (Prabhu et al., 2019) and (c) SCAN (ours). The green/red bounding boxes denote the true/false classification.

state-of-the-art FSL algorithms proposed in the computer vision area: S2M2_R (Mangla et al., 2020) and NegMargin (Liu et al., 2020). They both follow the transfer-learning training procedure. To learn the powerful feature encoder on base class set, S2M2_R (Mangla et al., 2020) incorporates self-supervised loss and Manifold-Mixup, while NegMargin (Liu et al., 2020) utilizes large-margin cosine softmax loss with a negative number as a margin. To combine our SCAN with these existing approaches, we append the projection head \mathbf{z}_θ and the cluster classifier $C(\cdot | \mathbf{W}_{cluster}^{base})$ to the penultimate layer of the original S2M2_R and NegMargin frameworks. Also, two losses $\mathcal{L}_{cluster}$ and \mathcal{L}_{purity} are added to the original training loss of the two methods. The experimental results are summarized in Tables 4 and 5. We find that our SCAN branch boosts the accuracy of S2M2_R (Mangla et al., 2020) and NegMargin (Liu et al., 2020) methods by around 1%-3%.

4.4. Ablation Study

4.4.1. Backbone architectures

Besides WRN-28-10 architecture, we also test the performance of SCAN on Conv4, Conv6, ResNet18 and ResNet34 to verify its robustness on different backbone networks. We compare it with the Baseline (Chen et al., 2019) method which trains the model with only \mathcal{L}_{class} and the results are shown in Table 6. We find that SCAN can boost the performance consistently under various backbones. The improvements are around 2%~4% when using shallow networks Conv4 and Conv6, while the increases are 2%~5% when implementing deeper networks, like ResNet18, Resnet34, and WRN-28-10. This is probably because of the overfitting problem on the base set. That is, when the backbone architectures become deeper, we obtain higher accuracy on simple convolutional networks, like Conv4 and Conv6, than those with deeper structures, like

ResNet18 and Resnet34. The performance also achieves best when we extend the width of the network, i.e., Wide ResNet (WRN).

4.4.2. Effectiveness of each component

To separately validate the effects of three parts in SCAN, i.e., a class branch with standard cross-entropy loss \mathcal{L}_{class} , a clustering branch with only cluster loss $\mathcal{L}_{cluster}$, and purity loss \mathcal{L}_{purity} , we test their respective influences on the performances of the SD-198 dataset. Note that the purity loss is appended to the model only when the clustering branch exists as it is designed for clustering refinement. Table 7 summarizes the outcomes of three situations: with class branch only, with class and clustering branches excluding the purity loss, and with all three parts. Thus, we can draw the conclusion that both cluster loss and purity loss produce positive effects on novel class inferences. Moreover, to show the ability of purity loss to refine clustering results on the base class set, we further define *cluster error rate* to measure the quality of all the sub-clusters, which refers to the percentage of samples in the wrong clusters accounting for the whole data. To compute cluster error rate, we sum the number of items with different class labels from the major examples for each cluster, and divide the total training set size. After applying purity loss, the cluster error rate decreases significantly.

4.4.3. Visualization of feature distribution in base classes

To demonstrate the ability of our proposed SCAN framework to learn the sub-cluster structures, we show the feature distribution in the base classes of the SD-198 dataset by t-SNE visualization (Van der Maaten and Hinton, 2008). Figure 6 displays the results of feature distributions of 20 base classes in the SD-198 dataset. In Figure 6 a), the features extracted without the clustering branch are well classified by the class labels,

Table 8: The calculation of inter-class variance D_{inter} , intra-class variance D_{intra} and discriminative function ϕ on the novel classes of SD-198 and Derm7pt datasets.

Dataset	Method	$D_{inter}(C)$	$D_{intra}(C)$	$\phi(C)$
SD-198	Baseline (Chen et al., 2019)	0.265644	0.250569	1.060161
	SCAN (ours)	0.259522	0.226078 ↓	1.147933 ↑
Derm7pt	Baseline (Chen et al., 2019)	0.109657	0.365394	0.302087
	SCAN (ours)	0.103585	0.244574 ↓	0.424906 ↑

since the cross-entropy loss inclines to align the same class features and minimize any intra-class dissimilarities. Compared to the baseline, our proposed method is more capable of dispersing the features within a class and forming several potential clusters, shown in Figure 6 b). Although the boundaries between classes become blurred, the sub-cluster information is reflected by the feature distributions. Moreover, as we do not assign a specific number to them, the numbers of clusters for each class are variant (mainly in one to three) which indicates distinct distributions for different classes. Therefore, our SCAN framework gives the freedom to the model to learn more flexible clusters for various classes. In Figure 7 (1 - 6), we demonstrate the grouping results from one to three clusters by listing the parts of images with corresponding features in the t-SNE visualization figure. For the one-cluster classes, the whole class is considered to be a union group because of the high similarity between items. As shown in Figure 7 (1 and 2), the inflected regions of these two classes are located in almost the same site (the chin area for class Perioral Dermatitis, and the nose area for class Rhinophyma). Accordingly, the characters of these types of skin diseases tend to be unified. For the two-cluster and three-cluster classes, the diverse behaviors of the same category of disease are mainly owing to different body locations, for instance, the back and the feet areas in the two clusters of class Psoriasis displayed in Figure 7 (3). To sum up, our proposed method can learn the extra knowledge about the cluster arrangement within a class by an additional unsupervised clustering branch and two restricted losses.

4.4.4. Discriminability analysis on novel class features

The clustering branch improves the learning of feature embedding on the base classes, while the role on the novel set still needs to be verified. We utilize the inter-class $D_{inter}(C)$ and intra-class variance $D_{intra}(C)$ applied in (Liu et al., 2020) and the discriminative function $\phi(C)$ defined in (Mika et al., 1999) to quantify the discriminability of deep features on the novel set. The larger value of $\phi(C)$ indicates that the extracted features are more distinguishable for unseen classes. We denote $C = \{c_1, c_2, \dots, c_k\}$ as k novel classes, k is 70 for the SD-198

dataset and 5 for the Derm7pt dataset. In each novel class $c_m, m \in \{1, 2, 3, \dots, k\}$, we have a set of labelled data denoted as $\{(x_i, y_i) | y_i = j\}$. Then, we have the specific formula for $D_{inter}(C)$, $D_{intra}(C)$ and $\phi(C)$:

$$D_{inter}(C) = \frac{1}{k(k-1)} \sum_{m=1}^k \sum_{n=1, n \neq m}^k \|\mu(c_m) - \mu(c_n)\|_2^2 \quad (8)$$

$$D_{intra}(C) = \frac{1}{k} \sum_{m=1}^k \left(\frac{1}{|c_m|} \sum_{(x_i, y_i) \in c_m} \left\| \frac{f_\theta(x_i)}{\|f_\theta(x_i)\|} - \mu(c_m) \right\|_2^2 \right) \quad (9)$$

$$\phi(C) = \frac{D_{inter}(C)}{D_{intra}(C)}, \quad (10)$$

where $\mu(c_m)$ is the mean of the L2-normalized feature vectors of class c_m .

The calculation of $D_{inter}(C)$, $D_{intra}(C)$ and $\phi(C)$ on the novel classes of SD-198 and Derm7pt dataset are reported in Table 8. After adding the clustering branch, the inter-class variances on the novel data set are almost invariant while the intra-class variances drop significantly which leads to an increase in the value of discriminative function $\phi(C)$. Therefore, we draw the conclusion that the feature representations learned by our proposed model on the base classes have a better ability to generalize and adapt to the unseen classes.

4.4.5. Visualization of classification results on novel classes

To compare the episodic predictions among various methods, we display three examples for the 5-way, 1-shot experiment of (a) Baseline (Chen et al., 2019), (b) PCN (Prabhu et al., 2019) and (c) SCAN (ours) in Figure 8. The first row are the sampled support set images, showing one example per class from total five classes. The yellow bonding box denotes the ground truth category for query images. The following three rows display the results of query images for three methods. The green/red boxes indicate the correct/incorrect predictions on the target class in the support set. In general, our method produces more accurate predictions on the listed query set than others, especially in episode (1) and (2) of Figure 8. Except

for the correct decisions on examples with high similarity to the support image, for example, the first three images in (1), our method can handle the cases that are distinguishable from the given support item, such as the last two columns in (1), and the first and the fifth columns in (2). Nonetheless, the wrong prediction on the third column in episode (3) indicates that the performance might be affected by large inter-class similarity, since the third query image is more similar to the support image from the first class than the image sampled from the same class.

5. Conclusion

In this paper, we present a novel Sub-Cluster Aware Network (SCAN) for rare skin disease classification. According to our key insights, skin disease datasets have existing latent sub-groups within a class. Therefore, our proposed SCAN effectively learns the intrinsic sub-cluster structures of skin disease via a well-designed dual branch framework and three additive losses. The results tested on two public skin image datasets show that our method surpasses other state-of-the-art methods by around 4% for 1-shot and 2~3% for 5-shot scenarios.

References

- Chen, D., Chen, Y., Li, Y., Mao, F., He, Y., Xue, H., 2021. Self-supervised learning for few-shot image classification, in: ICASSP 2021-2021 IEEE International Conference on Acoustics, Speech and Signal Processing (ICASSP), IEEE. pp. 1745–1749.
- Chen, W.Y., Liu, Y.C., Kira, Z., Wang, Y.C.F., Huang, J.B., 2019. A closer look at few-shot classification. arXiv preprint arXiv:1904.04232 .
- Chung, B.H.Y., Chau, J.F.T., Wong, G.K.S., 2021. Rare versus common diseases: a false dichotomy in precision medicine. *NPJ Genomic Medicine* 6, 1–5.
- Çiçek, Ö., Abdulkadir, A., Lienkamp, S.S., Brox, T., Ronneberger, O., 2016. 3d u-net: learning dense volumetric segmentation from sparse annotation, in: International conference on medical image computing and computer-assisted intervention, Springer. pp. 424–432.
- Cohen, T., Welling, M., 2016. Group equivariant convolutional networks, in: International conference on machine learning, PMLR. pp. 2990–2999.
- Dhillon, G.S., Chaudhari, P., Ravichandran, A., Soatto, S., 2019. A baseline for few-shot image classification. arXiv preprint arXiv:1909.02729 .
- Feng, R., Liu, X., Chen, J., Chen, D.Z., Gao, H., Wu, J., 2020. A deep learning approach for colonoscopy pathology wsi analysis: accurate segmentation and classification. *IEEE Journal of Biomedical and Health Informatics* 25, 3700–3708.
- Finn, C., Abbeel, P., Levine, S., 2017. Model-agnostic meta-learning for fast adaptation of deep networks, in: International Conference on Machine Learning, PMLR. pp. 1126–1135.
- Guo, Y., Codella, N.C., Karlinsky, L., Codella, J.V., Smith, J.R., Saenko, K., Rosing, T., Feris, R., 2020. A broader study of cross-domain few-shot learning, in: European Conference on Computer Vision, Springer. pp. 124–141.
- He, K., Zhang, X., Ren, S., Sun, J., 2016. Deep residual learning for image recognition, in: CVPR, pp. 770–778.
- Isensee, F., Jaeger, P.F., Kohl, S.A., Petersen, J., Maier-Hein, K.H., 2021. nnu-net: a self-configuring method for deep learning-based biomedical image segmentation. *Nature methods* 18, 203–211.
- Kawahara, J., Daneshvar, S., Argenziano, G., Hamarneh, G., 2018. Seven-point checklist and skin lesion classification using multitask multimodal neural nets. *IEEE journal of biomedical and health informatics* 23, 538–546.
- Li, X., Chen, H., Qi, X., Dou, Q., Fu, C.W., Heng, P.A., 2018. H-denseunet: hybrid densely connected unet for liver and tumor segmentation from ct volumes. *IEEE transactions on medical imaging* 37, 2663–2674.
- Li, X., Yu, L., Jin, Y., Fu, C.W., Xing, L., Heng, P.A., 2020. Difficulty-aware meta-learning for rare disease diagnosis, in: International Conference on Medical Image Computing and Computer-Assisted Intervention, Springer. pp. 357–366.
- Liu, B., Cao, Y., Lin, Y., Li, Q., Zhang, Z., Long, M., Hu, H., 2020. Negative margin matters: Understanding margin in few-shot classification, in: European Conference on Computer Vision, Springer. pp. 438–455.
- Van der Maaten, L., Hinton, G., 2008. Visualizing data using t-sne. *Journal of machine learning research* 9.
- Mahajan, K., Sharma, M., Vig, L., 2020. Meta-dermdiagnosis: few-shot skin disease identification using meta-learning, in:

- Proceedings of the IEEE/CVF Conference on Computer Vision and Pattern Recognition Workshops, pp. 730–731.
- Mangla, P., Kumari, N., Sinha, A., Singh, M., Krishnamurthy, B., Balasubramanian, V.N., 2020. Charting the right manifold: Manifold mixup for few-shot learning, in: Proceedings of the IEEE/CVF Winter Conference on Applications of Computer Vision, pp. 2218–2227.
- Medina, C., Devos, A., Grossglauser, M., 2020. Self-supervised prototypical transfer learning for few-shot classification. arXiv preprint arXiv:2006.11325 .
- Mika, S., Ratsch, G., Weston, J., Scholkopf, B., Mullers, K.R., 1999. Fisher discriminant analysis with kernels, in: Neural networks for signal processing IX: Proceedings of the 1999 IEEE signal processing society workshop (cat. no. 98th8468), Ieee. pp. 41–48.
- Nichol, A., Achiam, J., Schulman, J., 2018. On first-order meta-learning algorithms. arXiv preprint arXiv:1803.02999 .
- Phoo, C.P., Hariharan, B., 2020. Self-training for few-shot transfer across extreme task differences. arXiv preprint arXiv:2010.07734 .
- Prabhu, V., Kannan, A., Ravuri, M., Chaplain, M., Sontag, D., Amatriain, X., 2019. Few-shot learning for dermatological disease diagnosis, in: Machine Learning for Healthcare Conference, PMLR. pp. 532–552.
- Singh, R., Bharti, V., Purohit, V., Kumar, A., Singh, A.K., Singh, S.K., 2021. Metamed: Few-shot medical image classification using gradient-based meta-learning. Pattern Recognition , 108111.
- Snell, J., Swersky, K., Zemel, R.S., 2017. Prototypical networks for few-shot learning. arXiv preprint arXiv:1703.05175 .
- Sun, X., Yang, J., Sun, M., Wang, K., 2016. A benchmark for automatic visual classification of clinical skin disease images, in: European Conference on Computer Vision, Springer. pp. 206–222.
- Sung, F., Yang, Y., Zhang, L., Xiang, T., Torr, P.H., Hospedales, T.M., 2018. Learning to compare: Relation network for few-shot learning, in: Proceedings of the IEEE conference on computer vision and pattern recognition, pp. 1199–1208.
- Taghanaki, S.A., Zheng, Y., Zhou, S.K., Georgescu, B., Sharma, P., Xu, D., Comaniciu, D., Hamarneh, G., 2019. Combo loss: Handling input and output imbalance in multi-organ segmentation. Computerized Medical Imaging and Graphics 75, 24–33.
- Tian, Y., Wang, Y., Krishnan, D., Tenenbaum, J.B., Isola, P., 2020. Rethinking few-shot image classification: a good embedding is all you need?, in: Computer Vision–ECCV 2020: 16th European Conference, Glasgow, UK, August 23–28, 2020, Proceedings, Part XIV 16, Springer. pp. 266–282.
- Vinyals, O., Blundell, C., Lillicrap, T., Wierstra, D., et al., 2016. Matching networks for one shot learning. Advances in neural information processing systems 29, 3630–3638.
- Wang, X., Peng, Y., Lu, L., Lu, Z., Bagheri, M., Summers, R.M., 2017. Chestx-ray8: Hospital-scale chest x-ray database and benchmarks on weakly-supervised classification and localization of common thorax diseases, in: Proceedings of the IEEE conference on computer vision and pattern recognition, pp. 2097–2106.
- Wang, Y., Chao, W.L., Weinberger, K.Q., van der Maaten, L., 2019. SimpleShot: Revisiting nearest-neighbor classification for few-shot learning. arXiv preprint arXiv:1911.04623 .
- Wang, Y., Zhou, L., Yu, B., Wang, L., Zu, C., Lalush, D.S., Lin, W., Wu, X., Zhou, J., Shen, D., 2018. 3d auto-context-based locality adaptive multi-modality gans for pet synthesis. IEEE transactions on medical imaging 38, 1328–1339.
- Wu, Z., Efros, A.A., Yu, S.X., 2018. Improving generalization via scalable neighborhood component analysis, in: Proceedings of the European Conference on Computer Vision (ECCV), pp. 685–701.
- Yang, S., Liu, L., Xu, M., 2021. Free lunch for few-shot learning: Distribution calibration. arXiv preprint arXiv:2101.06395 .
- Yu, L., Wang, S., Li, X., Fu, C.W., Heng, P.A., 2019. Uncertainty-aware self-ensembling model for semi-supervised 3d left atrium segmentation, in: International Conference on Medical Image Computing and Computer-Assisted Intervention, Springer. pp. 605–613.
- Yuan, P., Mobiny, A., Jahanipour, J., Li, X., Cicalese, P.A., Roysam, B., Patel, V.M., Dragan, M., Nguyen, H.V., 2020. Few is enough: task-augmented active meta-learning for brain cell classification, in: International Conference on Medical Image Computing and Computer-Assisted Intervention, Springer. pp. 367–377.

Zagoruyko, S., Komodakis, N., 2016. Wide residual networks. arXiv preprint arXiv:1605.07146 .

Zhang, D., Jin, M., Cao, P., 2020. St-metadiagnosis: Meta learning with spatial transform for rare skin disease diagnosis, in: 2020 IEEE International Conference on Bioinformatics and Biomedicine (BIBM), IEEE. pp. 2153–2160.

Zhu, W., Li, W., Liao, H., Luo, J., 2021. Temperature network for few-shot learning with distribution-aware large-margin metric. *Pattern Recognition* 112, 107797.

Zhu, W., Liao, H., Li, W., Li, W., Luo, J., 2020. Alleviating the incompatibility between cross entropy loss and episode training for few-shot skin disease classification, in: International Conference on Medical Image Computing and Computer-Assisted Intervention, Springer. pp. 330–339.